

# Hidden fully-compensated ferrimagnetism

San-Dong Guo\*

*School of Electronic Engineering, Xi'an University of Posts and Telecommunications, Xi'an 710121, China*

Incorporating zero-net-magnetization magnets that exhibit spin-splitting into spintronics delivers key advantages: faster switching dynamics, greater immunity to destabilizing fields, lower power consumption, and markedly improved overall efficiency. The collinear magnets with net-zero magnetization and spin-splitting mainly include altermagnet and fully-compensated ferrimagnet, which provide possibility to achieve hidden spin polarization (HSP) with net-zero spin polarization in total but non-zero local spin polarization. In addition to proposal of hidden altermagnetism, we hereby introduce this concept of hidden fully-compensated ferrimagnetism, where the total spin polarization is zero, but either of the two inversion-partner sectors possesses fully-compensated ferrimagnetism with non-zero local spin polarization in the real space. By the first-principle calculations, we predict that  $PT$ -bilayer  $\text{CrMoC}_2\text{S}_6$  is a possible hidden fully-compensated ferrimagnet, showing fully-compensated ferrimagnetic HSP, which can be separated and observed by an out-of-plane external electric field. Our works provide a class of hidden spin-polarized materials that facilitates the advancement of spintronics.

**Introduction.**— Hidden spin polarization (HSP) has been proposed in centrosymmetric nonmagnetic systems, where the global crystal symmetry forces spin degeneracy, but the noncentrosymmetric individual sector can produce visible spin-splitting effects in the real space[1]. With the help of spin-orbit coupling (SOC), the Dresselhaus-type and Rashba-type [2, 3] momentum-dependent spin-splitting can exist in noncentrosymmetric individual sector. Subsequently, a number of layered bulk materials have been theoretically predicted and experimentally observed, which can exhibit HSP[4–10]. The HSP has also been observed in two-dimensional (2D)  $\text{PtSe}_2$  by the measurement of spin- and angle-resolved photoemission spectroscopic[11]. More hidden physical effects have also been proposed, for example hidden orbital polarization and hidden Berry curvature[12–14]. In addition to Dresselhaus-type and Rashba-type, the spin-splitting can also exist in magnetic materials without the assistance of SOC, such as ferromagnets, ferrimagnets and altermagnets[15–19], which provide the possibility to construct individual sector of HSP system. Here, we focus on the collinear magnets with net-zero magnetization, because they possess advantages of faster switching dynamics, greater insensitivity to destabilizing fields, reduced power consumption and so on[20].

The altermagnet and fully-compensated ferrimagnet of collinear magnets encompass not only net-zero magnetization but also spin-splitting. Unlike conventional antiferromagnetism, the two sublattices of altermagnetism are connected by rotational/mirror transformation rather than by translation or inversion, which can exhibit alternating spin-splitting of  $d$ -,  $g$ -, or  $i$ -wave symmetry in Brillouin zone (BZ)[15]. Various altermagnetic materials have been revealed both experimentally and theoretically[21], and even multifunctional altermagnets have been proposed, like valley-polarized and antiferroelectric altermagnets[22–27]. The fully-compensated ferrimagnet represents a unique class of ferrimagnetic ma-

terials characterized by net-zero magnetization[28–30]. Recently, the importance of 2D fully-compensated ferrimagnet is also emphasized[31], which broadens low-dimensional spintronic materials. The two sublattices of fully-compensated ferrimagnetism are related by null symmetry, and its net-zero magnetization is due to gap-guaranteed spin quantization in one spin channel[31]. The spin-splitting of fully-compensated ferrimagnetism is because the magnetic atoms with opposite spin polarization locate in the different environment, which can also be used to explain the spin-splitting of altermagnetism (the different environment is produced by the orientation of surrounding atoms arrange.)[32]. Unlike conventional antiferromagnet, both altermagnet and fully-compensated ferrimagnet with net-zero magnetization can produce anomalous Hall/Nernst effect and magneto-optical Kerr effect[21, 31].

Recently, hidden altermagnetism has been proposed, and the system possesses  $PT$  symmetry (the joint symmetry of space inversion symmetry ( $P$ ) and time-reversal symmetry ( $T$ )) with total net-zero spin polarization, but either of the two inversion-partner sectors possesses altermagnetism with local non-zero spin polarization in the real space[33]. In this work, we extend this idea and further propose the concept of hidden fully-compensated ferrimagnetism: the system with  $PT$  symmetry consists of two separate fully-compensated ferrimagnetic inversion partners, and it possesses net-zero spin polarization in total, but either of the two inversion-partner sectors has local non-zero spin polarization in the real space. Although symmetry analysis suggests that antiferromagnets hosting HSP can be classified into six types, the ref.[34] does not explicitly state that individual sector can be a fully-compensated ferrimagnet (From a symmetry perspective, ferrimagnetism is often subsumed under ferromagnetism.).

By first-principles calculations,  $PT$ -symmetric bilayer  $\text{CrMoC}_2\text{S}_6$  is used as a example to elaborate hidden

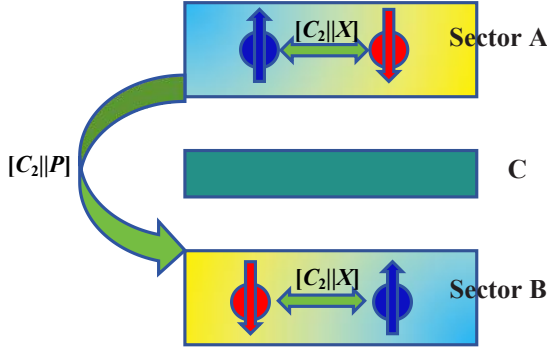


FIG. 1. (Color online) For  $PT$ -antiferromagnet, the system consists of sector A, sector B and C, and the C plane contains the inversion center, which separates the unit cell into sector A and B. The sector A and B with net-zero magnetization are connected by the  $[C_2||P]$ . The spin-up and spin-down magnetic atoms of sector A and B are connected by  $[C_2||X]$ . If  $X$  denotes null symmetry operation, the sector A and B are fully-compensated ferrimagnets, and the system is referred to as hidden fully-compensated ferrimagnetism. If  $X$  stands for rotation or mirror symmetry operation, the sector A and B are altermagnets, and the system is called hidden altermagnetism.

fully-compensated ferrimagnetism, and an out-of-plane external electric field is applied to separate local fully-compensated ferrimagnetic spin-splitting. In fact,  $PT$ -symmetric bilayer can form a large class of hidden fully-compensated ferrimagnet, as long as fully-compensated ferrimagnet is used as the building block. Both hidden fully-compensated ferrimagnetism and hidden altermagnetism can provide alternate ideas to explore stable low-power spintronic devices.

**Concept of hidden fully-compensated ferrimagnetism.**— For  $PT$ -antiferromagnet, the global degeneracy or no spin-splitting is constrained by symmetry:  $E_{\uparrow}(k) = PTE_{\uparrow}(k) = PE_{\downarrow}(-k) = E_{\downarrow}(k)$ . However, the local spin polarization can be achieved by introducing the degree of freedom of the 'layer' in the real space. In this study, we propose the concept of *Hidden fully-compensated ferrimagnetism* (Figure 1). The system consists of sector A, B and C, and the C plane contains the inversion center, separating the unit cell into sector A and B. The sector A and B possess net-zero magnetization, and they are connected by the  $[C_2||P]$  (The  $C_2$  is the two-fold rotation perpendicular to the spin axis in the spin space.), producing a  $PT$ -antiferromagnet. The spin-up and spin-down magnetic atoms of sector A and B are connected by  $[C_2||X]$  (The  $X$  means null symmetry operation in the lattice space). These means that A and B are fully-compensated ferrimagnet. If  $X$  stands for rotation or mirror symmetry operation, the sector A and B are altermagnets, and the system is called hidden altermagnetism[33].

The difference between hidden altermagnetism and hidden fully-compensated ferrimagnetism is shown in

	Altermagnet	Fully-compensated ferrimagnet
Sector A		
Sector B		
Total		

FIG. 2. (Color online) The sector A and B are altermagnets (fully-compensated ferrimagnets), and they show inverse momentum-dependent (global) spin-splitting, giving rise to at least two-fold degenerate energy bands of  $PT$ -antiferromagnet. The spin-up and spin-down channels are depicted in blue and red, and the gray means spin degeneracy.

Figure 2. For hidden altermagnetism, the sector A and B are altermagnets, giving rise to inverse momentum-dependent spin-splitting, such as  $d$ -wave,  $g$ -wave and  $i$ -wave symmetry[15]. For hidden fully-compensated ferrimagnetism, the sector A and B are composed of fully-compensated ferrimagnet, producing inverse global spin-splitting of  $s$ -wave symmetry. For both cases, the energy bands of the whole system is at least doubly degenerate.

Searching for realistic hidden fully-compensated ferrimagnet is difficult, but bilayer stacking engineering provides a general way to achieve hidden fully-compensated ferrimagnetism. By a similar way of building hidden altermagnet[33], we can construct hidden fully-compensated ferrimagnet by taking fully-compensated ferrimagnetic monolayer as the basic building unit. The fully-compensated ferrimagnetic monolayer can be obtained from  $PT$ -antiferromagnet and altermagnet by removing the link symmetry between magnetic atoms with opposite spin polarization using external electric field, built-in electric field and isovalent alloying[31, 32, 35–39], such as fully-compensated ferrimagnetic  $\text{CrMoC}_2\text{S}_6$ ,  $\text{Cr}_2\text{CHCl}$ ,  $\text{Fe}_2\text{CFCl}$ ,  $\text{Mn}_2\text{ClI}$ ,  $\text{V}_2\text{F}_7\text{Cl}$  and so on. In the bilayer system, a perpendicular electric field  $E$  can make the fully-compensated ferrimagnetism localized on each layer to be observable, producing the layer-locked anomalous Hall/Nernst effect and magneto-optical Kerr effect. The spin/layer order can be reversed by reversing the direction of the electric field. Here, we take  $\text{CrMoC}_2\text{S}_6$  monolayer as the basic building unit to illustrate the concept of hidden fully-compensated ferrimagnetism.

**Computational detail.**— We perform spin-polarized first-principles calculations within density functional theory (DFT) [40], as implemented in Vienna ab initio simulation package (VASP)[41–43] by using the projector augmented-wave (PAW) method. The gener-

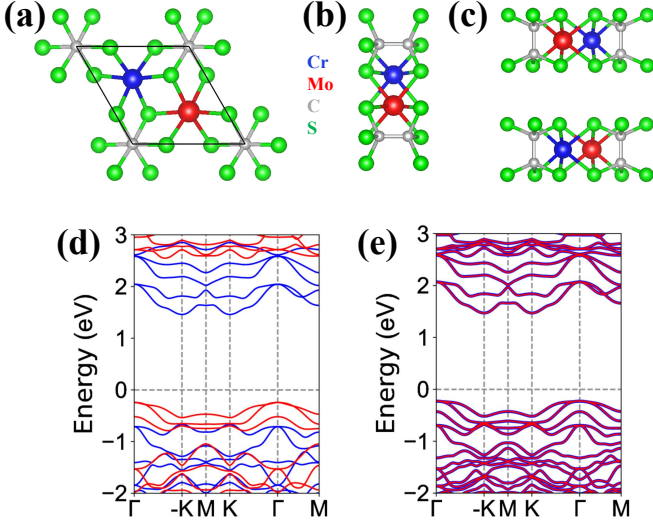


FIG. 3. (Color online) The top (a) and side (b) views of the crystal structure and energy band structures (d) of monolayer  $\text{CrMoC}_2\text{S}_6$ ; The side (c) view of the crystal structure and energy band structures (e) of  $PT$ -bilayer  $\text{CrMoC}_2\text{S}_6$ . In (a, b, c), the blue, red, gray and green balls represent Cr, Mo, C and S atoms, respectively. In (d, e), the spin-up and spin-down channels are depicted in blue and red.

alized gradient approximation (GGA) of Perdew, Burke, and Ernzerhof (PBE)[44] as the exchange-correlation functional is adopted. The kinetic energy cutoff of 500 eV, total energy convergence criterion of  $10^{-7}$  eV, and force convergence criterion of less than  $0.001 \text{ eV} \cdot \text{\AA}^{-1}$  are set to obtain the accurate results. We add Hubbard correction with  $U=3.00 \text{ eV}$ [36] for  $d$ -orbitals of both Cr and Mo atoms within the rotationally invariant approach proposed by Dudarev et al[45]. A slab model with a vacuum thickness of more than  $15 \text{ \AA}$  along  $z$  direction is used to avoid interlayer interactions. We sample BZ with a  $13 \times 13 \times 1$  Monkhorst-Pack  $k$ -point meshes for structure relaxation and electronic structure calculations. The dispersion-corrected DFT-D3 method[46] is adopted to describe the van der Waals (vdW) interactions. We determine the magnetic orientation by calculating magnetic anisotropy energy (MAE):  $E_{MAE} = E_{SOC}^{\parallel} - E_{SOC}^{\perp}$ , where  $\parallel$  and  $\perp$  mean that spins lie in the plane and out-of-plane.

**Material realization.**— The  $\text{CrMoC}_2\text{S}_6$  monolayer has been proved to be dynamically, mechanically and thermally stable[35, 36], and its crystal structures are shown in Figure 3 (a, b), crystallizing in the  $P312$  space group (No.149) without spatial inversion symmetry. The magnetic ground state of  $\text{CrMoC}_2\text{S}_6$  shows that Cr and Mo have opposite spin polarization in one primitive cell with total net-zero magnetization, and they cannot be symmetrically connected, giving rise to fully-compensated ferrimagnetism. In fact, the fully-compensated ferrimagnetic  $\text{CrMoC}_2\text{S}_6$  can be obtained

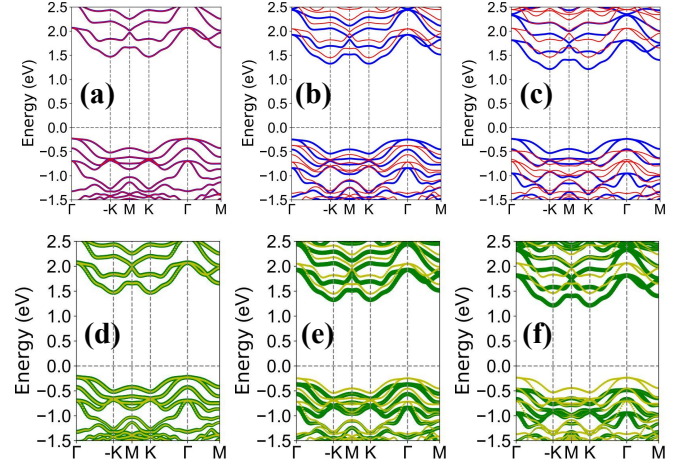


FIG. 4. (Color online) For bilayer  $\text{CrMoC}_2\text{S}_6$ , the energy band structures (a, b, c) with layer-characteristic projection (d, e, f) at representative  $E=+0.00, +0.02$  and  $+0.04 \text{ V/\AA}$ . In (a, b, c), the spin-up and spin-down channels are depicted in blue and red. In (d, e, f), the yellow and green represent lower- and upper-layer characters.

by substituting one Cr of  $PT$ -antiferromagnetic  $\text{Cr}_2\text{C}_2\text{S}_6$  with Mo via isovalent alloying. The optimized theoretical lattice constants are  $a=b=5.714 \text{ \AA}$  by using GGA+ $U$  method. The energy band structures of  $\text{CrMoC}_2\text{S}_6$  are plotted in Figure 3 (d) without SOC, which shows a large spin-splitting around the Fermi energy level due to  $d$  orbital mismatch between Cr and Mo atoms. The  $\text{CrMoC}_2\text{S}_6$  shows an indirect gap with conduction band bottom (CBM)/valence band maximum (VBM) at K/ $\Gamma$  point, and the  $\text{CrMoC}_2\text{S}_6$  is also a bipolar ferrimagnetic semiconductor because of VBM and CBM from different spin channels. The total magnetic moment of  $\text{CrMoC}_2\text{S}_6$  per unit cell is strictly  $0.00 \mu_B$ , and the magnetic moments of Cr and Mo atoms are  $2.88 \mu_B$  and  $-2.34 \mu_B$ , respectively.

Next, we build  $P$ -symmetric bilayer  $\text{CrMoC}_2\text{S}_6$ , and its crystal structures are shown in Figure 3 (c), crystallizing in the  $P3$  space group (No.147) with spatial inversion symmetry. The intralayer AFM and interlayer FM (AFM1), and intralayer AFM and interlayer AFM (AFM2) configurations (see FIG.S1[47]) are constructed to determine the magnetic ground state of bilayer  $\text{CrMoC}_2\text{S}_6$ , and the AFM1 magnetic configuration satisfies  $PT$  symmetry. Calculated results show that bilayer  $\text{CrMoC}_2\text{S}_6$  possesses AFM1 ground state, which is  $1.32 \text{ meV}$  per unit cell lower than that of AFM2 case. This ensures that bilayer  $\text{CrMoC}_2\text{S}_6$  is globally spin degenerate, producing hidden fully-compensated ferrimagnetism. In general, the electron correlation of  $4d$  electrons is weak than that of  $3d$  electrons. To ensure that bilayer  $\text{CrMoC}_2\text{S}_6$  exhibits hidden fully-compensated ferrimagnetism, it should adopt the AFM1 ordering. Therefore, the different  $U(\text{Cr, Mo})$  values are also considered



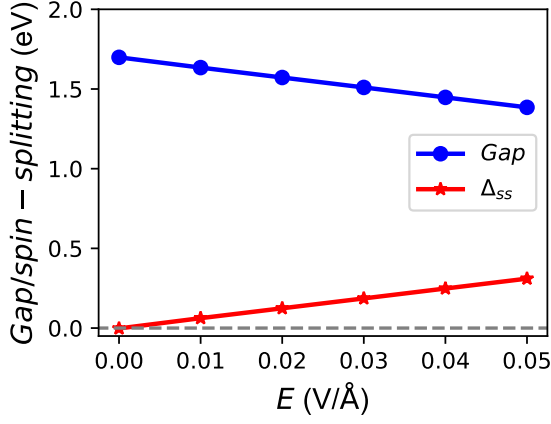


FIG. 5. (Color online) For bilayer  $\text{CrMoC}_2\text{S}_6$ , the energy band gap ( $\text{Gap}$ ) and the spin-splitting ( $\Delta_{ss}$ ) of CBM (The energy difference between the first and second conduction bands at  $-K/K$  point) as a function of electric field  $E$ .

to calculate the energy difference between AFM2 and AFM1 ordering. From  $U(3, 2)$  to  $U(3, 3)$  to  $U(4, 3)$ , the energy difference between AFM2 and AFM1 ordering changes from 2.47 meV to 1.32 meV to 1.71 meV, and these positive values confirm the reliability of our results. By GGA+ $U$  with AFM1 ordering, the optimized lattice constants  $a=b=5.686$  Å is slightly smaller than that of monolayer. The calculated MAE is  $247\mu\text{eV}/\text{unit cell}$ , implying the out-of-plane easy magnetization axis of bilayer  $\text{CrMoC}_2\text{S}_6$ . The energy band structures are plotted in Figure 3 (e) without SOC, which shows an indirect bandgap semiconductor with VBM/CBM at  $K/\Gamma$  point. Calculated results show that every band is doubly degenerate due to  $PT$  symmetry.

Electric field is an effective way to break  $P$  symmetry of  $PT$ -antiferromagnet, and then can lift the spin degeneracy[38]. An external electric field along the  $z$ -direction is applied to bilayer  $\text{CrMoC}_2\text{S}_6$ , and the magnetic ground state is determined under  $+z$  electric field ( $E=0.00-0.05$  V/Å) by the energy difference between AFM2 and AFM1 ordering. Based on FIG.S2[47], the AFM1 ordering is always ground state within considered  $E$  range. The MAE as a function of  $E$  is shown in FIG.S3[47], and the positive MAE confirms that the easy axis of bilayer  $\text{CrMoC}_2\text{S}_6$  is always out-of-plane within considered  $E$  range.

Without including SOC, the energy band structures with spin- and layer-characteristic projection at representative  $E=+0.00, +0.02$  and  $+0.04$  V/Å are plotted in Figure 4. With applied electric field, it is clearly seen that there is spin-splitting of  $s$ -wave symmetry, which is due to layer-dependent electrostatic potential caused by out-of-plane electric field. The layer-characteristic projection along with spin-polarized character shows that each layer possesses fully-compensated ferrimagnetic spin-splitting. The valence and conduction bands in proximity to the

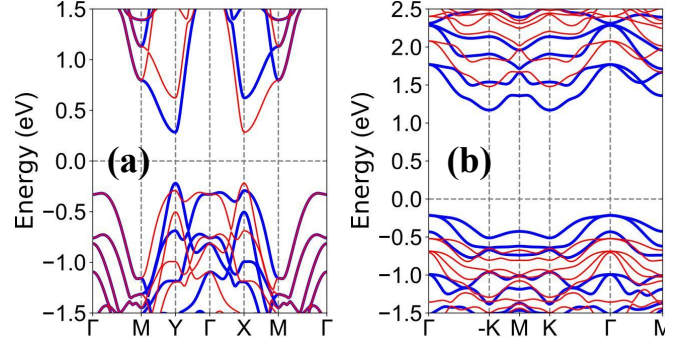


FIG. 6. (Color online) The energy band structures of hidden altermagnetic bilayer  $\text{Cr}_2\text{SO}$  (a) and hidden fully-compensated ferrimagnetic bilayer  $\text{CrMoC}_2\text{S}_6$  (b) at  $E=+0.05$  V/Å.

Fermi level exhibit identical spin characteristics but possess distinct layer attributes. Due to identical spin characteristics of VBM and CBM, a sufficiently strong electric field can induce a half-metallic state. The real-space segregation of spin-splitting make hidden fully-compensated ferrimagnetism to be observed experimentally. When the direction of electric field is reversed, the order of spin- or layer-splitting is also reversed (see FIG.S4[47]).

The energy band gap along with the spin-splitting of CBM as a function of electric field  $E$  are plotted in Figure 5. A linear relationship is evident between gap/spin-splitting and electric field, and the gap decreases, while the spin-splitting increases with increasing  $E$ . The spin-splitting of CBM can be approximately estimated by  $eEd$  with  $e$  and  $d$  being the electron charge and the inter-layer distance of two magnetic layers[25]. For example  $E=+0.04$  V/Å, the estimated spin-splitting is approximately 250 meV with the  $d$  being 6.24 Å, which is very close to the DFT result of 248 meV.

**Discussion and Conclusion.**— In experiment, both hidden altermagnetism and hidden fully-compensated ferrimagnetism with local spin-splitting can be observed by using spin- and angle-resolved photoemission spectroscopy (ARPES) measurements, which has been used in measuring HSP effect of nonmagnetic materials[7–11]. The difference between hidden altermagnetism and hidden fully-compensated ferrimagnetism lies in the symmetry of local spin-splitting. To illustrate the difference, the energy band structures of hidden altermagnetic bilayer  $\text{Cr}_2\text{SO}$ [33] and hidden fully-compensated ferrimagnetic bilayer  $\text{CrMoC}_2\text{S}_6$  at  $E=+0.05$  V/Å are plotted in Figure 6. Bilayer  $\text{Cr}_2\text{SO}$  shows momentum-dependent spin-splitting with  $d$ -wave symmetry, while bilayer  $\text{CrMoC}_2\text{S}_6$  manifests global spin-splitting with  $s$ -wave symmetry.

The degree of freedom of the “layer” in real space for hidden magnetism can produce layer-locked phenomena of anomalous Hall/Nernst effect, nonrelativistic spin-polarized currents and the magneto-optical Kerr effect possessed by both fully-compensated ferrimagnet and

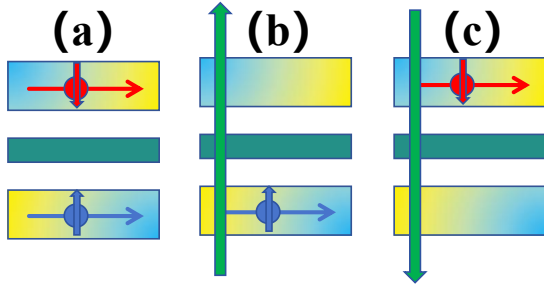


FIG. 7. (Color online) For hidden fully-compensated ferrimagnet, for example bilayer  $\text{CrMoC}_2\text{S}_6$ , (a): without out-of-plane electric field, a hole doping can lead to spin current in both upper and lower layers; (b): with an out-of-plane electric field, an appropriate hole doping results in the presence of spin current only in the lower layer; (c): by reversing the direction of the electric field, the spin current is confined to the upper layer. In (b) and (c), the green arrow represents the vertical electric field.

altermagnet[21, 31]. In the absence of an out-of-plane electric field, the introduction of carriers enables both layers to become functional (Figure 7 (a)). When the electric field is applied, an appropriate carrier doping can make just one layer play a role (Figure 7 (b)). By reversing the direction of the electric field, another layer will activate (Figure 7 (c)). Hidden altermagnet and hidden fully-compensated ferrimagnet constitute a special class of net-zero magnetization magnet, which can advance the development of spintronic devices with high immunity to magnetic field disturbance.

In summary, we propose the concept of hidden fully-compensated ferrimagnetism with the global spin degeneracy and the local spin-splitting of  $s$ -wave symmetry, namely that the individual sectors are fully-compensated ferrimagnets with net-zero magnetization. By the first-principles calculations, we demonstrate hidden fully-compensated ferrimagnetism by an extensive study of  $PT$ -symmetric bilayer  $\text{CrMoC}_2\text{S}_6$ , and a vertical electric field can be used to separate and detect the local spin-splitting. Our findings provide future directions for HSP research in magnets with global and local net-zero magnetization, and motivate more theoretical and experimental works to explore other relevant physical effects.

This work is supported by Natural Science Basis Research Plan in Shaanxi Province of China (2025JC-YBMS-008). We are grateful to Shanxi Supercomputing Center of China, and the calculations were performed on TianHe-2. We thank Prof. Guangzhao Wang for providing VASP software and helpful discussions.

\* sandongyuwang@163.com

[1] X. Zhang, Q. Liu, J. W. Luo, A. J. Freeman and A. Zunger, Hidden spin polarization in inversion-symmetric

- bulk crystals, *Nat. Phys.* **10**, 387 (2014).
- [2] G. Dresselhaus, Spin-orbit coupling effects in zinc blende structures, *Phys. Rev.* **100**, 580 (1955).
- [3] Y. A. Bychkov and E. I. Rashba, Oscillatory effects and the magnetic susceptibility of carriers in inversion layers, *J. Phys. C Solid State Phys.* **17**, 6039 (1984).
- [4] C. Cheng, J. T. Sun, X. R. Chen, and S. Meng, Hidden spin polarization in the 1T-phase layered transition-metal dichalcogenides  $\text{MX}_2$  ( $M = \text{Zr, Hf}$ ;  $X = \text{S, Se, Te}$ ), *Sci. Bull.* **63**, 85 (2018).
- [5] Q. Liu, X. Zhang, H. Jin, K. Lam, J. Im, A. J. Freeman, and A. Zunger, Search and design of nonmagnetic centrosymmetric layered crystals with large local spin polarization, *Phys. Rev. B* **91**, 235204 (2015).
- [6] T. T. Debela, and H. S. Kang, Phase polymorphism and electronic structures of  $\text{TeSe}_2$ , *J. Mater. Chem. C* **6**, 10218 (2018).
- [7] E. Razzoli, T. Jaouen, M. L. Mottas, B. Hildebrand, G. Monney, A. Pisoni, S. Muff, M. Fanciulli, N. C. Plumb, V. A. Rogalev, V. N. Strocov, J. Mesot, M. Shi, J. H. Dil, H. Beck, and P. Aebi, Selective Probing of Hidden Spin-Polarized States in Inversion-Symmetric Bulk  $\text{MoS}_2$ , *Phys. Rev. Lett.* **118**, 086402 (2017).
- [8] K. Zhang, S. Zhao, Z. Hao, S. Kumar, E. F. Schwier, Y. Zhang, H. Sun, Y. Wang, Y. Hao, X. Ma, C. Liu, L. Wang, X. Wang, K. Miyamoto, T. Okuda, C. Liu, J. Mei, K. Shimada, C. Chen, and Q. Liu, Observation of Spin-Momentum-Layer Locking in a Centrosymmetric Crystal, *Phys. Rev. Lett.* **127**, 126402 (2021).
- [9] G. Gatti, D. Gosálbez-Martnez, S. Roth, M. Fanciulli, M. Zacchigna, M. Kallane, K. Rossnagel, C. Jozwiak, A. Bostwick, E. Rotenberg, A. Magrez, H. Berger, I. Vobornik, J. Fujii, O. V. Yazyev, M. Grioni, and A. Crepaldi, Hidden bulk and surface effects in the spin polarization of the nodal-line semimetal  $\text{ZrSiTe}$ , *Commun. Phys.* **4**, 54 (2021).
- [10] H. J. Qian, X. Zhang, C. M. Liu, Q. Jiang, W. J. Liu, H. M. Zha, D. Y. Wang, X. P. Shen, M. Ye, Y. F. Guo, and S. Qiao, Layer-locked spin states revealed in the centrosymmetric nodal-line semimetal  $\text{HfSiS}$ , *Phys. Rev. B* **104**, 035145 (2021).
- [11] W. Yao, E. Wang, H. Huang, K. Deng, M. Yan, K. Zhang, K. Miyamoto, T. Okuda, L. Li, Y. Wang, H. Gao, C. Liu, W. Duan, and S. Zhou, Direct observation of spin-layer locking by local Rashba effect in monolayer semiconducting  $\text{PtSe}_2$  film, *Nat. Commun.* **8**, 14216 (2017).
- [12] S. Guan, J. X. Xiong, Z. Wang, and J. W. Luo, Progress of hidden spin polarization in inversion-symmetric crystals, *Sci. China-Phys. Mech. Astron.* **65**, 237301 (2022).
- [13] J. H. Ryoo and C. H. Park, Hidden orbital polarization in diamond, silicon, germanium, gallium arsenide and layered materials, *NPG Asia Mater.* **9**, e382 (2017).
- [14] R. Chen, H. P. Sun, M. Gu, C. B. Hua, Q. Liu, H. Z. Lu and X. C. Xie, Layer Hall effect induced by hidden Berry curvature in antiferromagnetic insulators, *Nat Sci Rev.* **11**, nwac140 (2024).
- [15] L. Šmejkal, J. Sinova and T. Jungwirth, Beyond conventional ferromagnetism and antiferromagnetism: A phase with nonrelativistic spin and crystal rotation symmetry, *Phys. Rev. X* **12**, 031042 (2022).
- [16] I. Mazin, Altermagnetism: a new punch line of fundamental magnetism, *Phys. Rev. X* **12**, 040002 (2022).
- [17] S. Hayami, Y. Yanagi and H. Kusunose, Momentum-

- Dependent Spin Splitting by Collinear Antiferromagnetic Ordering, *J. Phys. Soc. Jpn.* **88**, 123702 (2019).
- [18] S. Hayami, Y. Yanagi and H. Kusunose, Bottom-up design of spin-split and reshaped electronic band structures in antiferromagnets without spin-orbit coupling: Procedure on the basis of augmented multipoles, *Phys. Rev. B* **102**, 144441 (2020).
  - [19] S. Hayami and H. Kusunose, Essential role of the anisotropic magnetic dipole in the anomalous Hall effect, *Phys. Rev. B* **103**, L180407 (2021).
  - [20] S. S. Fender, O. Gonzalez and D. K. Bediako, Altermagnetism: A Chemical Perspective, *ChemRxiv*. 2024; doi:10.26434/chemrxiv-2024-bst3p.
  - [21] L. Bai, W. Feng, S. Liu, L. Šmejkal, Y. Mokrousov, and Y. Yao, Altermagnetism: Exploring New Frontiers in Magnetism and Spintronics, *Adv. Funct. Mater.* 2409327 (2024).
  - [22] Y. Liu, J. Yu and C. C. Liu, Twisted Magnetic Van der Waals Bilayers: An Ideal Platform for Altermagnetism, *Phys. Rev. Lett.* **133**, 206702 (2024).
  - [23] R. He, D. Wang, N. Luo, J. Zeng, K. Q. Chen and L. M. Tang, Nonrelativistic Spin-Momentum Coupling in Antiferromagnetic Twisted Bilayers, *Phys. Rev. Lett.* **130**, 046401 (2023).
  - [24] S. D. Guo, Y. Liu, J. Yu and C. C. Liu, Valley polarization in twisted altermagnetism, *Phys. Rev. B* **110**, L220402 (2024).
  - [25] R. W. Zhang, C. X. Cui, R. Z. Li, J. Y. Duan, L. Li, Z. M. Yu and Y. G. Yao, Predictable gate-field control of spin in altermagnets with spin-layer coupling, *Phys. Rev. Lett.* **133**, 056401 (2024).
  - [26] S. D. Guo, X. S. Guo and G. Wang, Valley polarization in two-dimensional tetragonal altermagnetism, *Phys. Rev. B* **110**, 184408 (2024).
  - [27] X. Duan, J. Zhang, Z. Zhang, I. Žutić and T. Zhou, Antiferroelectric Altermagnets: Antiferroelectricity Alters Magnets, arXiv:2410.06071 (2024).
  - [28] H. van Leuken and R. A. de Groot, Half-Metallic Antiferromagnets, *Phys. Rev. Lett.* **74**, 1171 (1995).
  - [29] H. Akai and M. Ogura, Half-Metallic Diluted Antiferromagnetic Semiconductors, *Phys. Rev. Lett.* **97**, 026401 (2006).
  - [30] S. Wurmehl, H. C. Kandpal, G. H. Fecher, and C. Felser, Valence electron rules for prediction of half-metallic compensated-ferrimagnetic behaviour of Heusler compounds with complete spin polarization, *J. Phys.: Condens. Matter* **18**, 6171 (2006).
  - [31] Y. Liu, S. D. Guo, Y. Li and C. C. Liu, Two-dimensional fully-compensated Ferrimagnetism, *Phys. Rev. Lett.* **134**, 116703 (2025).
  - [32] S. D. Guo, Y. L. Tao, G. Wang and Y. S. Ang, How to produce spin-splitting in antiferromagnetic materials, *J. Phys.: Condens. Matter* **36**, 215804 (2024).
  - [33] S. D. Guo, Hidden altermagnetism, *Front. Phys.* in press (2025).
  - [34] L. D. Yuan, X. Zhang, C. M. Acosta and A. Zunger, Uncovering spin-orbit coupling-independent hidden spin polarization of energy bands in antiferromagnets, *Nat. Commun.* **14**, 5301 (2023).
  - [35] L. Zhang, S. D. Guo, X. S. Guo and G. Zhu, The iso-valent alloying assisted anomalous valley Hall effect in a hexagonal antiferromagnetic monolayer, *J. Mater. Chem. C* **13**, 465 (2025).
  - [36] P. Wang, D. X. Wu, K. Zhang and X. J. Wu, Two-Dimensional Quaternary Transition Metal Sulfide  $\text{CrMoA}_2\text{S}_6$  ( $A = \text{C, Si, or Ge}$ ): A Bipolar Antiferromagnetic Semiconductor with a High Néel Temperature, *J. Phys. Chem. Lett.* **13**, 3850 (2022).
  - [37] D. C. Liang, S. D. Guo and S. Chen, Anomalous valley Hall effect in electric-potential-difference antiferromagnetic  $\text{Cr}_2\text{CHCl}$  monolayer, *Appl. Phys. Lett.* **125**, 242402 (2024).
  - [38] S. D. Guo, L. Zhang, Y. Zhang, P. Li and G. Wang, Large spontaneous valley polarization and anomalous valley Hall effect in antiferromagnetic monolayer  $\text{Fe}_2\text{CF}_2$ , *Phys. Rev. B* **110**, 024416 (2024).
  - [39] S. D. Guo and Y. S. Ang, Spontaneous spin splitting in electric potential difference antiferromagnetism, *Phys. Rev. B* **108**, L180403 (2023).
  - [40] P. Hohenberg and W. Kohn, Inhomogeneous Electron Gas, *Phys. Rev.* **136**, B864 (1964); W. Kohn and L. J. Sham, Self-Consistent Equations Including Exchange and Correlation Effects, *Phys. Rev.* **140**, A1133 (1965).
  - [41] G. Kresse, Ab initio molecular dynamics for liquid metals, *J. Non-Cryst. Solids* **193**, 222 (1995).
  - [42] G. Kresse and J. Furthmüller, Efficiency of ab-initio total energy calculations for metals and semiconductors using a plane-wave basis set, *Comput. Mater. Sci.* **6**, 15 (1996).
  - [43] G. Kresse and D. Joubert, From ultrasoft pseudopotentials to the projector augmented-wave method, *Phys. Rev. B* **59**, 1758 (1999).
  - [44] J. P. Perdew, K. Burke and M. Ernzerhof, Generalized gradient approximation made simple, *Phys. Rev. Lett.* **77**, 3865 (1996).
  - [45] S. L. Dudarev, G. A. Botton, S. Y. Savrasov, C. J. Humphreys, and A. P. Sutton, Electron-energy-loss spectra and the structural stability of nickel oxide: An LSDA+U study, *Phys. Rev. B* **57**, 1505 (1998).
  - [46] S. Grimme, S. Ehrlich and L. Goerigk, Effect of the damping function in dispersion corrected density functional theory, *J. Comput. Chem.* **32**, 1456 (2011).
  - [47] See Supplemental Material at [] for the magnetic configurations; the energy difference between AFM2 and AFM1 ordering vs  $E$ ; the MAE vs  $E$ ; the related energy band structures.